PERGAMON

International Journal of Heat and Mass Transfer 44 (2001) 4465–4473

International Journal of HEAT and MASS TRANSFER

www.elsevier.com/locate/ijhmt

Numerical modeling and experimental investigation on the characteristics of molten pool during laser processing

L.X. Yang, X.F. Peng *, B.X. Wang

Department of Thermal Engineering, Tsinghua University, Beijing 100084 People's Republic of China

Received 11 September 2000; received in revised form 26 February 2001

Abstract

The article illustrates melting processes in fixed meshes, based on mixture continuity equations, momentum equations and energy equations for both liquid and solid phases by introducing scalar of liquid fraction and applying source-based method. The model was applied to laser processing of AISI 304 stainless steel. The effects of heat conduction, Marangoni flow and thermal buoyancy on melting process and shape of molten pool were analyzed and physical fundament of laser processing were evidenced. Compared to the experimental outcome, the proposed model and numerical techniques are validated.

Keywords: Melting; Laser; Marangoni flow; Phase change

1. Introduction

High energy density beam (HEDB) processing technology is a special processing technology taking high energy density beam (laser beam, electronic beam or plasma) as heat sources, which includes welding, incision, punching, spray paint, surface treatment, etch and fine machining, etc. After experiencing a half-centurial exploration, HEDB processing technology presents an accelerating development trend in 1980s. The technology has been considered as a highlight developing area of manufacture industry, one of underpinning industries, in critical technology layout of *Ninth five-year plan* in China. The fundamental research of HEDB processing technology involves many sciences, such as Heat and Mass Transfer, Hydrodynamics, Material and Computer Science, presenting multi-science and inter-disciplinary characteristics. So far, however, much attention is not paid to it. Usually in order to gain good processing outcome, many times of iterant experiments should be conducted to obtain a series of adaptable parameters. Also, there is still a lack of theoretical analyses for basic aspects from large amounts of laser-processing experimental data. Apparently, research on flow characteristics of molten body, such as shape of molten pool, temperature gradient, local cooling rate and condensed crystal structure, etc., is highly necessary for further understanding and mastering the principle of phase change and formation of condensation structure. Prompt and accurate analytical method will analytically instruct selection and control of technical parameters.

Formation and development of molten pool is a typical problem of solid–liquid phase change. A large body of publications was contributed to understand solid–liquid phase change transport phenomenon employing both analytical methods and numerical modeling in the last several decades. In late 1970s, E.M. Sparrow, etc. [1,2] begun to account for effects of convection on phase change processes. Using method of small disturbance, Peng et al. [3] gave explanation of mechanism of initial molten pool and effects of Marangoni flow on the pool forming and developing. As a rapid development of computer technology and numerical methods, recently more and more investigations focused on modeling some dominant characteristics of molten pool by numerical techniques [4,5]. The numerical methods can mainly be divided into two types, fixed mesh method and transient mesh method. Transient mesh method is normally used in open

* Corresponding author. Tel.: +86-10-6278-9751; fax: +86-10-6277-0209.

E-mail address: pxf-dte@mail.tsinghua.edu.cn (X.F. Peng).

0017-9310/01/$ - see front matter
PII: S0017-9310(01)00086-2

Nomenclature

a_i	percentage of active substance in samples
A_σ	gradient constant of surface tension, N (m K)$^{-1}$
C_P	specific heat at constant pressures, J (kg K)$^{-1}$
D	constant related to morphology of mushy region
f_L	liquid volume fraction
f_S	solid volume fraction
h_q	laser energy density, W (m^2)$^{-1}$
h_C	combined heat transfer coefficient, W (m^2 K)$^{-1}$
ΔH_0	standard absorbing heat, J (kg mole)$^{-1}$
k_l	constant related to entropy of segregation
R_g	gas constant, J (kg mole K)$^{-1}$
T_L	liquidus temperature, K
T_S	solidus temperature, K
T	temperature, K
U	mixing velocity m s^{-1}
V_X	x-directional velocity component, m s^{-1}
V_Z	z-directional velocity component, m s^{-1}

Greek symbols

β	coefficient of thermal expansion, K^{-1}
Γ_S	surface excess at saturation, J (kg mole m^2)$^{-1}$
ε	surface emissivity
λ	thermal conductivity, W (m K)$^{-1}$
μ	dynamic viscosity, kg (m s)$^{-1}$
ρ	density, kg m^{-3}
σ	surface tension, N m^{-1}
σ_m	surface tension at melting point, N m^{-1}

literature, that is, to solve liquid zone and solid zone separately and couple them together using boundary conditions at liquid–solid interfaces. This method has a clear physical meaning. However, there are also some deficiencies, such as difficulties in the determining of initial molten pool in liquid zone and/or initial shape of molten pool inducing different numerical modeling result [6], difficulties in dealing with mushy zone of melted alloy, and large quantity of calculation work on iterant mesh generation. The above problems do not exist in fixed mesh method, but it does have difficulties in building model of mushy zone and calculation convergence. Lack of validation of related HEDB processing experimental outcome makes blocks in extending these numerical methods to practical industrial applications.

Present work illustrates solving condensation and melting processes in fixed meshes, based on unique Continuity Equations, Momentum Equations and Energy Equations for both liquid and solid phases. The unique conservation equations for two phases were developed by introducing scalar of liquid fraction and source-based method. The model was applied to laser processing of AISI 304 stainless steel. The effects of heat conduction, Marangoni flow and thermal buoyancy on melting process and shape of molten pool were thoroughly analyzed and the results were compared with the experimental substances, which validates the numerical techniques and reveals the fundamentals of laser processing.

2. Computational model

The processing of an AISI 304 stainless steel plate, having size of 10 mm × 8 mm × 2 mm, was considered in this work. Fig. 1 illustrates a schematic representation of physical model, together with geometry, coordinate and region on which laser beam directly acts.

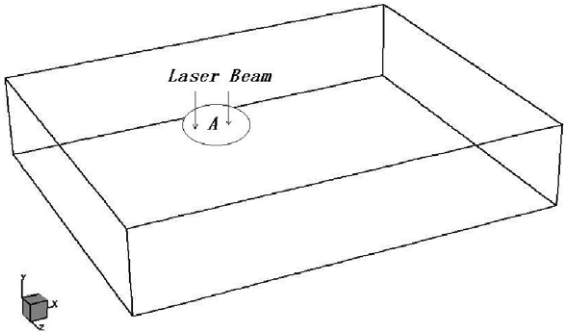

Fig. 1. Schematic representation of the numerical model.

The solid metal is melted by high energy density laser beam and forms an initial molten pool. Convective driving forces of melting liquid in the molten pool come from two sources. One is surface tension or Marangoni force due to the surface tension gradient along free interface, and the other is buoyancy force due to the density difference in the liquid metal pool. Melting process is actually a phase-change problem with moving boundary. Using liquid fraction scalar, introducing enthalpy source into energy conservation equation and Darcy source into momentum conservation equation, we set up unique continuity equation, momentum conservation equation and energy conservation equation, which enables solid region, liquid region and mushy region to be solved by fixed grids.

In building model, the following assumptions were introduced:

1. The flow is laminar and incompressible [7,8].
2. The thermal properties are independent of temperature (except for the temperature-dependent surface tension, heat capacity and thermal conductivity). Boussinesq approximation is adopted.
3. Distribution of laser energy density is parabolic.

2.1. Governing equations

The liquid fraction, f_L, is deduced from temperature, and is assumed to vary linearly between the solidus and liquidus temperatures. The solid and liquid fractions, f_S and f_L can be defined as

$$T > T_L, \quad f_L = 1, \tag{1}$$

$$T_S \leqslant T \leqslant T_L, \quad f_L = \frac{(T - T_S)}{(T_L - T_S)}, \tag{2}$$

$$f_S = 1 - f_L. \tag{3}$$

The continuity equations for the two phases expressed in terms of solid and liquid fractions, f_S and f_L, are

$$\frac{\partial}{\partial t}(\rho_L f_L) + \nabla \cdot (\rho_L U_L f_L) = \dot{m}_{LS}, \tag{4}$$

$$\frac{\partial}{\partial t}(\rho_S f_S) + \nabla \cdot (\rho_S U_S f_S) = \dot{m}_{LS}. \tag{5}$$

If densities ρ_s and ρ_L are equal, Eqs. (4) and (5) can be combined and the inter-phase mass transfer term is eliminated. The unique (mixture) continuity equation is then

$$\frac{\partial \rho}{\partial t} + \nabla \cdot (\rho U) = 0, \tag{6}$$

where the mixture velocity is,

$$U = f_L U_L + f_S U_S. \tag{7}$$

Similarly, combining the momentum equations for the solid and liquid phases, a mixture momentum equation is derived as

$$\frac{\partial \rho U}{\partial t} + \nabla \cdot (\rho U \otimes U) = -\nabla \cdot P + \nabla \cdot (\mu \nabla U) - \frac{\mu}{K} U. \tag{8}$$

The final term of the momentum equation represents the resistance to the flow of liquid through the mushy region. It is in the form of a Darcy-like resistant source, and tends to zero as the liquid volume fraction in its end. So, the mixture velocity approaches to that of the solid. The permeability, K, is related to the liquid volume fraction via the Kozeny–Carman [9] equation,

$$K = f_L^3/[D(1 - f_L)^2], \tag{9}$$

where the constant D is dependent upon the morphology of mushy region or particular solidifying material. In this study it was taken as 10^{10} m^{-2}.

The unique enthalpy equation for the melting material is again obtained by adding the separate enthalpy equations for the solid and liquid phases,

$$\frac{\partial}{\partial t}\rho H + \nabla \cdot \rho U H = \nabla \cdot \lambda \nabla T - \rho_L \left(\frac{\partial f_L}{\partial t}\right). \tag{10}$$

The last term on the right-hand side of the enthalpy equation represents the transient evolution of latent heat. The mixture enthalpy, H, is the weighted enthalpy of the solid and liquid and is expressed as

$$H = f_L H_L + f_S H_S. \tag{11}$$

2.2. Boundary conditions

2.2.1. Flow conditions on the free surface

At the free surface of melted pool, Region A shown in Fig. 1, the surface tension or Marangoni-driven flow is described by

$$-\mu \frac{\partial V_X}{\partial n} = \frac{d\sigma}{dT}\frac{\partial T}{\partial X}, \tag{12}$$

$$-\mu \frac{\partial V_Z}{\partial n} = \frac{d\sigma}{dT}\frac{\partial T}{\partial Z}. \tag{13}$$

In this study, the surface tension is a function of surface temperature and activity of species in the solution. The following relationship is employed [10]:

$$\sigma(T) = \sigma_m - A_\sigma (T - T_m) - R_g T \Gamma_S \ln(1 + K a_i), \tag{14}$$

$$K = k_l + \exp\left(-\frac{\Delta H_0}{R_g T}\right). \tag{15}$$

where A_σ is a constant, σ_m surface tension at melting point, R_g gas constant, Γ_S surface excess at saturation, K absorb coefficient, ΔH_0 standard heat adsorption and a_i activity of species in the solution.

The temperature-dependent surface tension gradients for alloy with a surface-active element were obtained by differentiating Eq. (14) with respect to T as follows:

$$\frac{d\sigma}{dT} = -A_\sigma - R_g \Gamma_S \ln(1 + K a_i) - \frac{K a_i}{(1 + K a_i)}\frac{\Gamma_S H_0}{T}. \tag{16}$$

2.2.2. Boundary conditions on heated surface

In the experiments and numerical simulation conducted in present research, a laser beam, frequency 20 Hz, plus width 5 ms, average power 300 W, was utilized. According to these parameters and the parabolic distribution assumption, the laser heat flux density h_q applying on the region A could be calculated. The heat transfer boundary condition in region A was expressed as

$$h_q = -k\frac{\partial T}{\partial Y}. \tag{17}$$

At the other region of the metal heating surface except region A, the heat transfer boundary condition was used as the following equation:

$$h_C(T - T_\infty) = -\lambda\frac{\partial T}{\partial z}, \tag{18}$$

where h_C is a combined heat transfer coefficient for the radiative and convective boundary conditions. The h_C can be calculated from the relationship given by Goldak [11]:

$$h_C = 24.1 \times 10^{-4}\varepsilon T^{1.61}, \tag{19}$$

where ε is the emissivity of a body surface. A value of 0.9 is generally assumed for ε, as recommended for the hot rolled steel.

2.2.3. Boundary condition on other surfaces

At the sides and bottom of steel plate, the adiabatic wall boundary conditions were adopted.

3. Numerical techniques

3.1. Grids

Establishment of mixture government equations for the solid and liquid phases makes the whole metal plate solved using fixed grids. The heat source was assumed to be located at point P (3 mm, 2 mm, 5 mm), which is not the center of plate. Therefore, three-dimensional grids were used to investigate the influence of asymmetry of region applied by laser beam. The model used a $100 \times 25 \times 75$ variable rectangular grid system for numerical calculation. Fig. 2 represents $X - Z$ plane section grid. In order to improve the accuracy of calculation, a grid system of variable spacing was utilized, i.e., finer spacing near the heat source and coarser grid away from the point P. The minimum grid is 0.04 mm at X, Z directions, while 0.01 mm at Y direction.

3.2. Numerical scheme and solution procedure

The governing equations and boundary conditions set up in the present analysis were discredited and solved using SIMPLE-C algorithm.

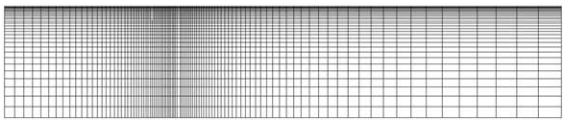

Fig. 2. X–Z plane mesh generation.

The simulation was a transient process, the initial temperature 400 K, and the time step 0.001 s. The next time step calculation continued until the relative residues of all physical variables less than 10^{-3} in the last time step simulation. The calculation was terminated at the end of five pluses. Totally 250 time steps were processed.

3.3. Two cases investigated

For getting more information from the simulation results to recognize well the flow and heat transfer mechanism in the molten and how the Marangoni force and buoyancy influence the forming and developing of molten pool shape, two simulating cases were carried out in present calculation.

Case 1: Only thermal conduction was considered for melting calculation, or the momentum equations were not solved.

Case 2: Marangoni force, buoyancy force and thermal conduction exist together.

In order to compare calculated results of two cases, all the calculating parameters are same, for example the same heat source, grids and solving time step, etc.

4. Discussion of numerical results

The numerical results of the two cases were compared, and particularly, the characteristics of molten temperature distribution, velocity field, and molten shape were discussed in detail. All of the data present here come from the results at time of 5 ms. It is emphatically an analysis about the flow influence on heat transfer and shape forming of molten pool.

4.1. Temperature profiles

Figure 3 illustrates the temperature distribution on heating surface. The cone-shaped profile of temperature is the sequence of parabolic heat energy distribution and heat conduction of solid steel. Because the heat source acting position is not symmetrical in X-axis direction (not at the center of the plate), the heat conduction is different on the two sides of molten pool along this direction. The asymmetry of temperature along X-axis consequently appears in Fig. 3. Fig. 3(a) is the result of 'case 1' and the maximal temperature is 2964 K. Fig. 3(b) is the result of 'case 2' and the maximal temperature is 2679 K. Owing to the Marangoni and thermal buoyancy forces, the higher temperature fluid flows from pool central outwards to solid–liquid interface. It decreases the maximum value of temperature and makes the more uniform temperature distribution on melting surface.

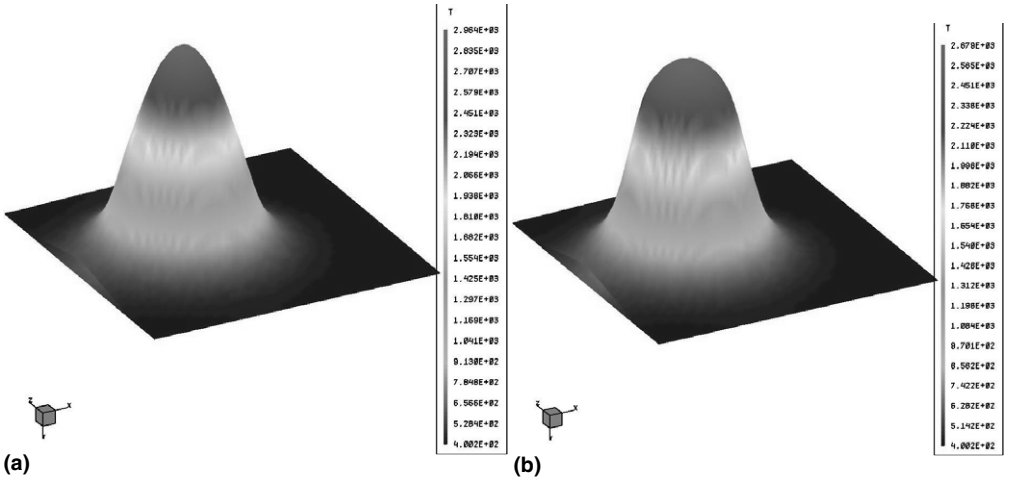

Fig. 3. Temperature distribution on heated surface: (a) case 1, (b) case 2.

4.2. Velocity field

For 'case 2', surface tension or Marangoni force and thermal buoyancy force enhance the heat transfer in molten pool by driving molten liquid flow. Figs. 4(a) and (b) depict the velocity vector and streamline on XY plane via the heating central, respectively. The molten liquid at the free surface flows from the central outwards to the solid–liquid interface and forms two vortexes in the molten pool. This is due to the negative value of surface tension gradient with respect to temperature because of a low level of 10 ppm sulfur content in steel. This flow pattern will make the molten pool shape become wider and shallower. The difference of thermal conduction conditions between two sides of pool results in the difference temperature and velocity distribution. Fig. 5 shows the surface velocity profile as a function of X-axial position. The maximum velocity is at position between pool central and right solid–liquid interface, about 0.285 m/s.

4.3. Shape of molten pool

Figure 6 illustrates the molten pool shape at XY plane via the heating central. Fig. 6(a) corresponding to the molten pool of 'case 1', the maximum pool width is 1.22 mm and pool depth is 0.235 mm. Fig. 6(b) corresponding to 'case 2', the maximum pool width is 1.35 mm and pool depth is 0.21 mm. According to previous analysis, the molten pool of 'case 2' is wider and shallower than that of 'case 1' due to the Marangoni and buoyancy flow. Therefore, in industry processing, we

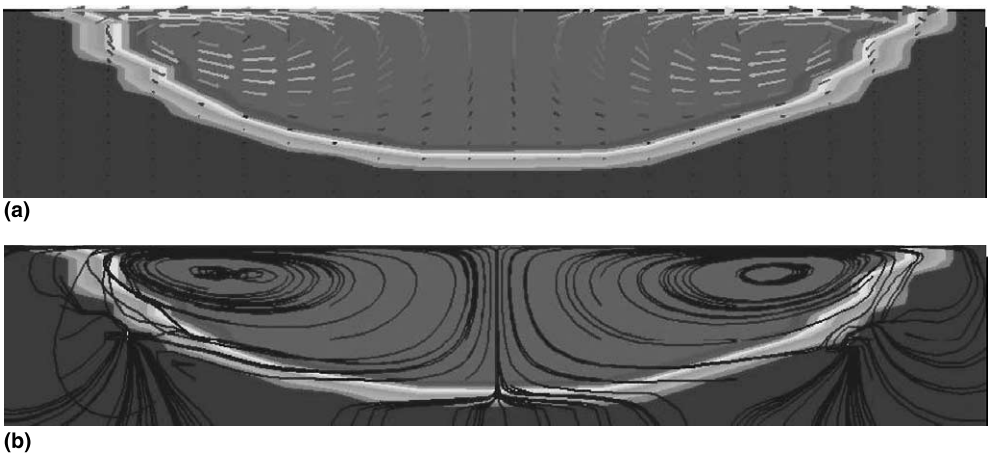

Fig. 4. Velocity distribution at X–Z middle plane: (a) vector plot, (b) streamline plot.

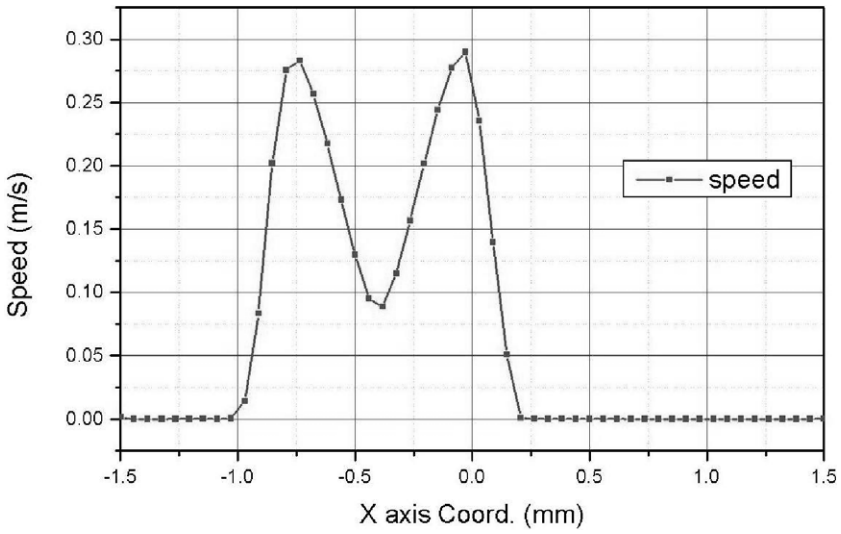

Fig. 5. Velocity distribution at the cross-section.

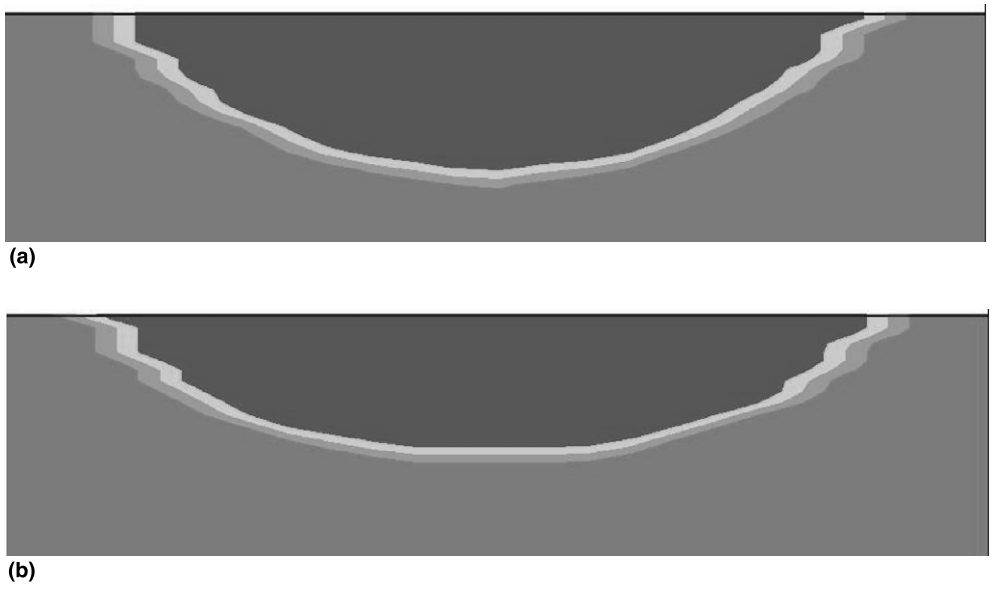

Fig. 6. Shapes of molten pool at the cross-section: (a) case 1, (b) case2.

can add some appropriate activity elements in process material to change its surface tension characters and get molten pool with large ratio of wide to depth.

5. Experiment and metallograph

5.1. Experiment apparatus and technique

The experimental investigation of punching and welding using YAG Solid Laser Apparatus was conducted to display the fundamental features, and also, to validate the theoretical predictions. The experimental rig is shown in Fig. 7, which was imported from Switzerland and with an advanced level of 1990s. The machine can provide a 500 W pulse laser beam and the digital control system is NUM760 system. It has an eight-shaft work platform. Six shafts are digital controlled, any four of which are cooperated, and the other two are manually operated to enlarge processing scope. It can be used for punching, incision, jointing and surface treatment. Main performance parameters

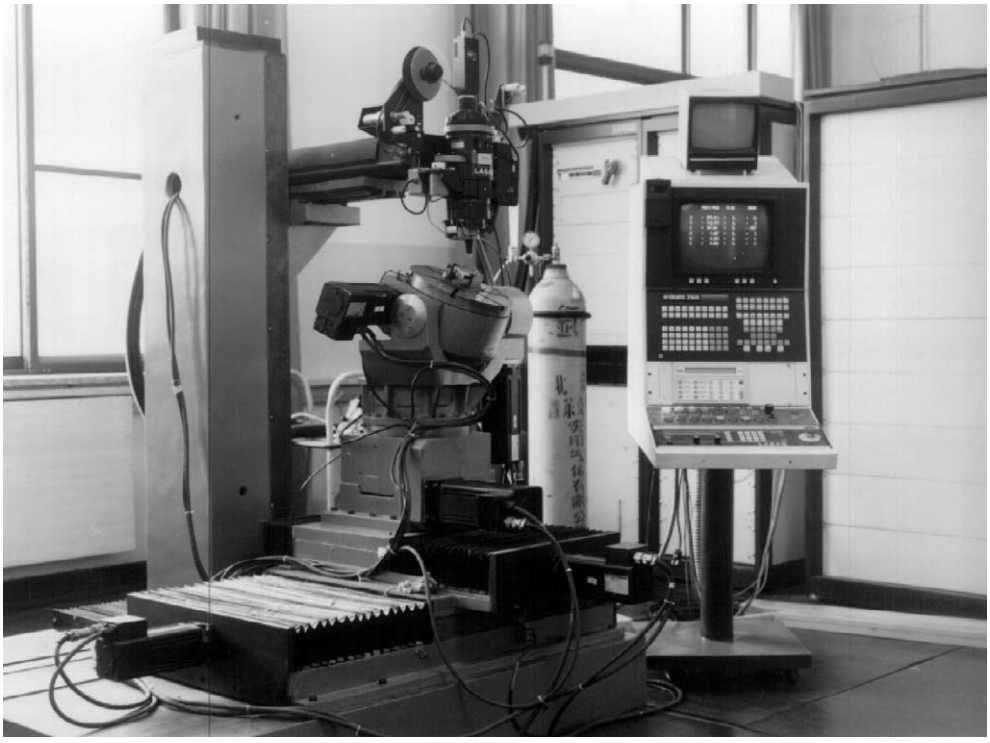

Fig. 7. Work platform of YAG laser apparatus.

include pulse bandwidth 0.1–20 ms, pulse frequency $\leqslant 300$ Hz and pulse energy ~ 50 J.

The experiment explored characteristics of three kinds of molten pool, molten pool of single-point jointing of different materials, initial molten pool in punching and welding molten pool. The sample segments were cut and rubbed to central cross-section, and metallograph was obtained by corrosion. Since metal crystal structure changed after condensation, we can clearly observe shape of the molten pool. From metallograph, effects of thermophysical properties and processing technique on the characteristics of molten pool can be analyzed. Since it is difficult to measure flowing velocity and temperature accurately in HEDB Processing Technology, the ultimate shape of molten pool is a good test of accuracy of numerical model.

Figure 8 illustrates metallograph of molten pool of single-point jointing of two different materials. In this

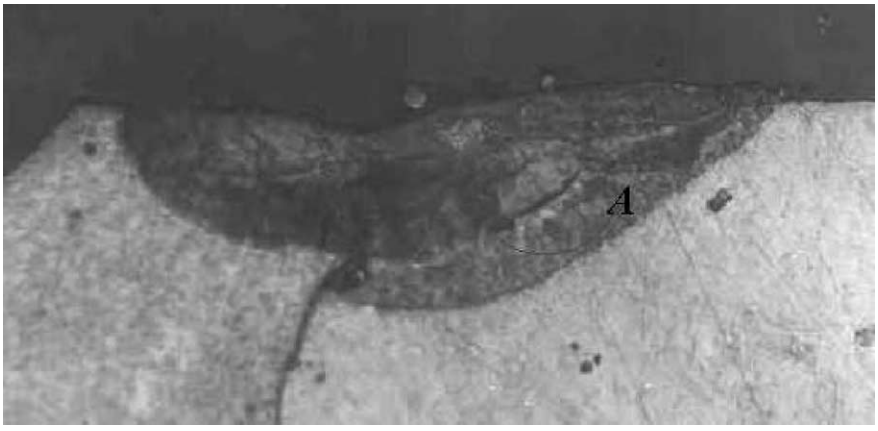

Fig. 8. Metallograph of molten pool for point jointing of two materials.

illustration, light zone is metal without phase change occurred during the processing. The left is stainless steel and the right side is copper. Properties of materials apparently have significant effects on shape of molten pool. Since heat capacity of copper is smaller than that of stainless steel (the ratio is 368:460), and heat conductivity is larger (the ratio is 398:15), the molten pool on the right side is wider and deeper. Due to existence of flow inside molten pool, partial melted steel flows from bottom of steel pool toward the zone of melted copper, and mixes, which changes properties of solidified materials. Zone A in the figure presents the flow mixing phenomena.

Figure 9 presents shape of molten pool of stainless steel applied with a single pulse with frequency of 20 Hz, width of 5 ms, average power 300 W. Light zone is metal without phase change occurred during the processing. Surface at the central part is a little lower than that at two sides. This point is actually corresponding to highest power density of laser beam. Energy density at the center was larger than 10^4 W/cm^2, calculated from performance parameters of laser beam given above, which makes a local temperature higher than boiling point of steel (2740°C for the actual experimental process. In the experiment liquid metal vaporization happened, and mass loss made the center a little bit lower. Interfacial shape of region A and B in the figure obviously exhibits the effects of flow on development of molten pool.

Figure 10 shows metallograph of center longitudinal cross section while the metal plate was continuously processed by a pulse of frequency 20 Hz, width 5 ms, average power 300 W with moving speed 1500 mm/min. Lines of A, B, C, etc. present development of internal shapes of molten pool. The corresponding positions of A_0, B_0, C_0 at the surface are highly dependent upon laser pulse parameters. The concave part following these points is corresponding to the pulse peak. The internal flowing in molten pool induced a fluctuation of the free surface and finally formed a waved shape while solidifying occurs. Apparently, fluctuation shape is the result of internal flowing, and tightly related to pulse parameters and material properties.

5.2. Comparison with numerical simulations

In Fig. 9, maximum width of molten pool is 1.4 mm, maximum depth 0.22 mm. The Section 4.2 interprets the asymmetry of molten pool shape, which is the result of different boundary conditions or due to existence of the

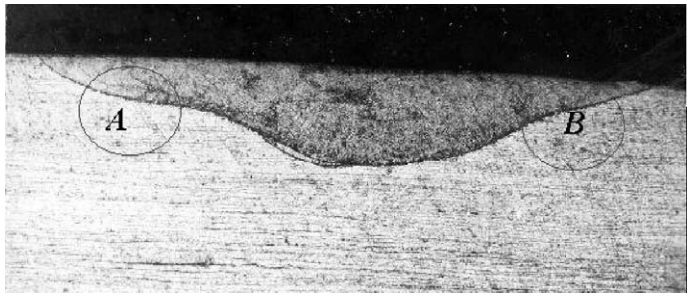

Fig. 9. Metallograph of initial molten pool in punching.

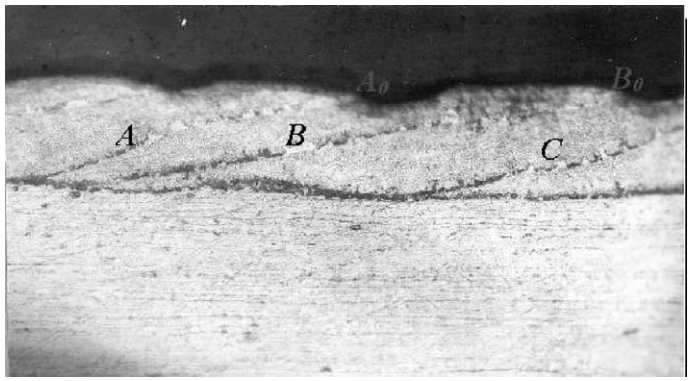

Fig. 10. Metallograph of molten pool of welting sew at cross-section.

difference in thermal boundary on the surface and in the metal plate. Comparing Fig. 9 with 'Case b' in Fig. 6, the simulation result shows a reasonably good agreement with the experimental outcome. In the area near to the border of solid–liquid interface, molten pool exhibits a little concave due to vortex by Marangoni Flow and thermal buoyancy, where flow turns around, brings hot fluid from the free surface down toward bottom and strengthens heat transfer. Numerical results show a fatter shape than the actual situation. The main reason is the assumption of parabolic distribution of laser energy density, which is Gauss distribution in fact. Meanwhile, the heat loss associated with metal vaporization was not included in the numerical simulations, which might be another factor making the prediction deviate from the experiments. Calculated results indicate that the temperature at central point is higher than boiling point of the steel, referring to Fig. 3, so some energy of laser beam will be carried out by vaporization. Compared with the experimental pictures, the numerical model developed is able to describe quite well the internal flow and transport phenomena in the molten pool of laser processing, and provides a very good understanding of the physical significance. Certainly, some modifications, such as energy loss caused by metal vaporization, should be included in future numerical model to improve the prediction.

6. Conclusions

A set of uniform governing equations including liquid and solid zone was developed to investigate and numerically simulate thawing and solidifying processes during laser processing. The model was applied to examine the laser processing of AISI304 stainless steel.

1. The flow and heat transfer characteristics in laser processing were successfully analyzed using the developed model and numerical simulation techniques. This will supply a powerful tool to further investigate more complex transport processes in a molten pool;
2. Marangoni Flow caused by different surface tension and thermal buoyancy significantly alter the characteristics of thawing and solidifying process, and make a molten pool wider and shallower;
3. The thermal properties of material have important effects on the transport phenomena in the molten pool, and consequently on the formation and shape of the molten pool.
4. The evaporation of metal occurring at power density center of a laser beam was noted to be serious for the surface formation during laser processing.

Acknowledgements

Project supported by the National Natural Science Foundation of China (Grant No. 59625612) and Doctoral Thesis Foundation of Tsinghua University.

References

[1] E.M. Sparrow, S.V. Patankar, S. Ramadhyani, Analysis of melting in the presence of natural convection in the melted region, ASME J. Heat Transfer 99 (1977) 520–526.
[2] E.M. Sparrow, R.R. Schmidt, J.W. Ramsey, Experiments on the role of natural convection in the melting of solid, ASME J. Heat Transfer 100 (1978) 11–16.
[3] X.F. Peng, X.P. Lin, D.J. Lee, Y. Yan, B.X. Wang, Effect of initial molten pool and Marangoni flow on solid melting, Int. J. Heat Mass Transfer 44 (2001) 457–470.
[4] B. Basu, J. Strnivasna, Numerical study of steady state laser melting problem, Int. J. Heat Mass Transfer 31 (1988) 2331–2338.
[5] M. Lacroix, Effect of buoyancy and surface tension forces on melting of a metal, Numer. Heat Transfer, Part A: Appl. 19 (1991) 101–115.
[6] X.P. Lin, X.F. Peng, B.X. Wang, D.M. Christopher, Influence of Marangoni flow on the melting process, Progr. Nat. Sci. 7 (1997) 616–623.
[7] M.E. Thompson, J. Szekely, The transient behaviors of weld pools with a deformed free surface, Int. J. Heat Mass Transfer 32 (1989) 1007–1019.
[8] R.T.C. Choo, J. Szekely, R.C. Westhoff, Modeling of high-current arcs with emphasis on free surface phenomena in the weld pool, Weld. J. Res. Supply (1990) 346–361.
[9] V.R. Voller, C.R. Swaminathan, General source-based method for solidification phase change, Numer. Heat Transfer, Part B 19 (1991) 175–189.
[10] T. Zacharia, S.A. David, J.M. Vitek, T. Debroy, Weld pool development during GTA and laser beam welding of type 304 stainless steel, Part I – theoretical analysis, Weld. J. Res. Supply (1989) 499–509.
[11] J. Goldak, Computer modeling of heat flow in welds, Metall. Trans. (1986) 17–26.